Colloids and Surfaces A: Physicochemical and Engineering Aspects 651 (2022) 129625

Contents lists available at ScienceDirect

Colloids and Surfaces A: Physicochemical and Engineering Aspects

journal homepage: www.elsevier.com/locate/colsurfa

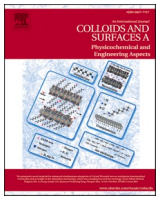

Effect of concentration of silica encapsulated ds-DNA colloidal microparticles on their transport through saturated porous media

Swagatam Chakraborty [a,*], Jan Willem Foppen [b,d], Jack F. Schijven [a,c]

[a] Environmental Hydrogeology Group, Department of Earth Sciences, Utrecht University, Princetonlaan 8a, 3584 CB Utrecht, the Netherlands
[b] Department of Water Sciences and Engineering, IHE-Delft, Institution for Water Education, Westvest 7, 2611 AX Delft, the Netherlands
[c] Department of Statistics, Informatics and Modelling, National Institute of Public Health and the Environment, P.O.Box 1, 3720 BA Bilthoven, the Netherlands
[d] Water Resource Section, Department of Civil Engineering and Geoscience, Delft University of Technology, Delft, the Netherlands

GRAPHICAL ABSTRACT

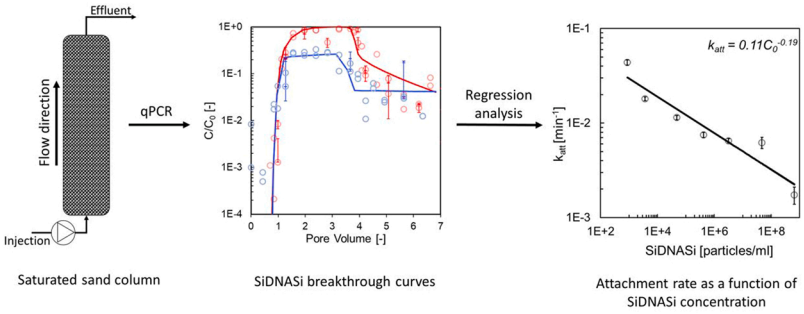

ARTICLE INFO

Keywords:
Silica encapsulated – silica core dsDNA particles
Injection concentration
Saturated porous media
Attachment rate
Single collector removal efficiency

ABSTRACT

We investigated the transport and retention kinetics of silica encapsulated – silica core double stranded DNA particles (SiDNASi) through 15 cm saturated quartz sand columns as a function of a wide range of colloid injection concentrations ($C_0 = 8.7 \times 10^2$ - 6.6×10^8 particles ml^{-1}). The breakthrough curves (BTCs) exhibited an overall 2-log increase of maximum relative effluent concentration with increasing C_0. Inverse curve fitting, using HYDRUS1D, demonstrated that a 1-site first order kinetic attachment (k_{att}) and detachment (k_{det}) model sufficed to explain the C_0-dependent SiDNASi retention behaviour. With increasing C_0, k_{att} log-linearly decreased, which could be expressed as an overall decrease in the single-collector removal efficiency (η). The decrease in η was likely due to increased electrostatic repulsion between aqueous phase- solid phase colloids, formation of shadow zones downstream of deposited colloids and removal of weakly attached colloids from the solid phase (quartz sand) attributing to increased aqueous phase-solid phase intercolloidal collisions as a function of increasing SiDNASi concentration. Our results implied, firstly, that the aqueous phase colloid concentration should be carefully considered in determining colloidal retention behaviour in saturated porous media. Secondly, colloidal transport and retention dynamics in column studies should not be compared without considering colloid influent concentration. Thirdly, our results implied that the applicability of SiDNASi as a conservative subsurface tracer was restricted, since transport distance and retention was colloid concentration dependent. However, the

* Corresponding author.
E-mail address: s.chakraborty@uu.nl (S. Chakraborty).

https://doi.org/10.1016/j.colsurfa.2022.129625
Received 28 April 2022; Received in revised form 28 June 2022; Accepted 29 June 2022
Available online 6 July 2022

uniqueness of the DNA sequences in SiDNASi imparts the advantage of concurrent use of multiple SiDNASi for flow tracking or porous media characterization.

1. Introduction

An understanding of the physicochemical processes governing the transport and retention of colloidal particles through saturated porous media is imperative due to their importance in carrying subsurface contaminants such as radionuclides, organic compounds, tracer elements [3,49], in-situ contaminated site remediation Fazeli Sangani, Owens, & Fotovat [25], use as hydrological tracers [51,93] or being contaminant themselves [36].

Physical and chemical factors, such as collector size, injection solution chemistry, colloidal size, flow velocity, have been widely documented to significantly influence subsurface transport of inorganic (e.g. fullerene, graphene oxide, latex, titanium dioxide, silica) or (bio)colloids (e.g. bacteria, viruses) (Fig. 1.1). The colloidal input concentration ranges used in these studies, however, vary over 10 orders of magnitude (Fig. 1.1) with little or no inter-study overlapping. This complicates comparing the outcomes and their applicability of the colloidal transport behaviour over a large spectrum of colloidal concentrations. In comparison with the physicochemical parameters mentioned, regardless of multiple researches indicating the significance of colloidal injection concentration on colloidal deposition and retention behaviour, a systematic investigation to this end is still limited. A careful consideration of colloidal injection concentration and its influence on the colloidal transport behaviour, therefore, is imperative. Additionally, implications of colloidal concentration dependent transport and retention kinetics could be even more significant when colloid facilitated contaminant or microorganism transport is considered [30,91], specifically when contaminant transport have been observed to be hindered or facilitated depending on colloidal concentration [61].

In light of that, a few studies [10,11,86,87] have investigated concentration dependent colloidal transport and retention behaviour under unfavourable deposition condition (in the presence of an energy barrier to deposition). Retention of colloids is generally explained as single collector removal efficiency (η), the product of concentration independent single collector contact efficiency (η_0) and single collector attachment efficiency (α), dealing with intercolloidal and colloid-collector grain interactions and subsequent attachment probability [85]. α and η_0 are individually influenced by chemical conditions of the experimental system, transport solution chemistry and collector surface properties [21,33]. However, while a few researchers considered a concentration independent η_0 and reported α to be concentration dependent due to increased probability of aggregate formation with increasing colloidal concentration resulting in higher deposition [62,64], Phenrat et al., [58] modified the equation for predicting η_0 considering that aggregation alters the effective particle size, an important variable for predicting η_0. A trend of a declining attachment coefficient (k_{att}) and a declining attachment efficiency (α) leading to decreased retention with increasing colloidal input concentrations (C_0) was observed by Wang et al., [87]. Lower mass retention with increasing input colloidal concentration was reported by Bradford and Bettahar [9] as well. Vitorge et al., [86], while investigating transport of colloids within a concentration range of $7.7 \times 10^8 - 2.9 \times 10^{12}$ particles/ml for four different colloidal sizes (110, 260, 450 and 660 nm) identified a critical injection concentration, below which k_{att} increased with injection concentration denoting the onset of blocking. Contrasting colloidal transport behaviour, where deposition and attachment increased with

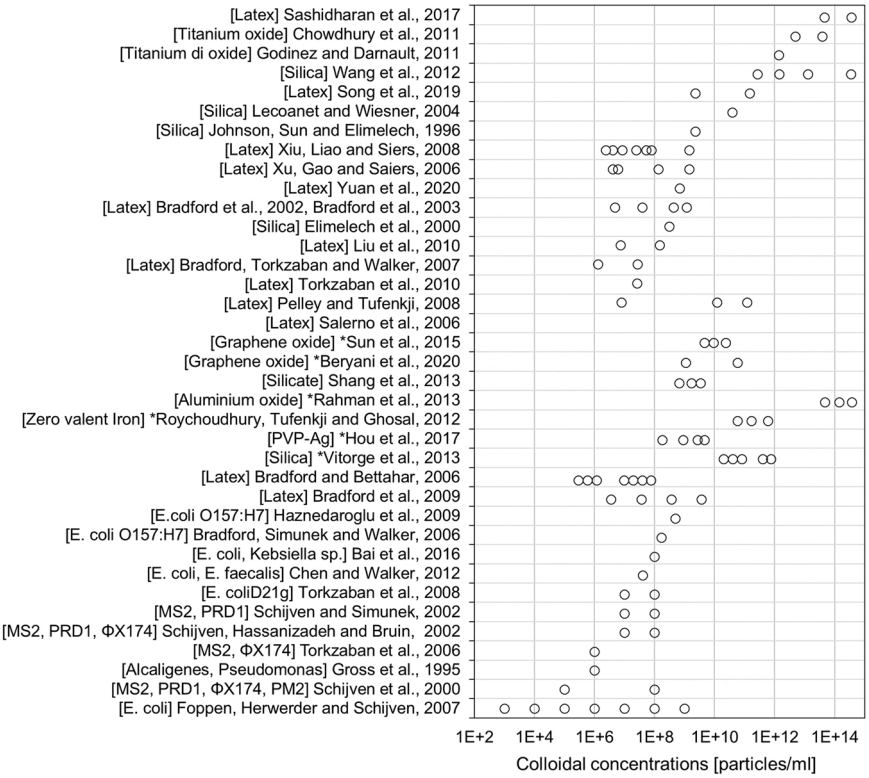

Fig. 1.1. Injection particle concentrations (particles/ml) used for different colloid transport experiment studies under saturated flow conditions. The approximated 'particles/ml' concentration for the asterisked (*) references were calculated by dividing the estimated particle weight (from particle diameter and particle density) by injected W/V concentration information provided by the authors [5,7,12,13,15,22,29, 32,35,37,43,57,67,68,70,71–73,81–83,89,92].

colloidal injection concentration due to formation of particle aggregates leading to pore plugging or straining, have also been reported [17,24,58]. However, such aggregation is only possible when the energy barrier between colloidal particles is diminished.

Enhanced colloidal mobility at higher injection concentrations or removal from solid matrix have also been attributed to inter-colloidal collisions resulting in aggregation or re-entrainment of weakly deposited colloids in the aqueous phase. Bradford et al., [10] hypothesized intercolloidal collision to be an important mechanism for removal or "knocking off" of solid phase particle, further supported by a micromodel observation. The authors considered η_0 to be concentration independent and the relative reduction in aqueous-to-solid phase colloidal mass transfer with increasing C_0 was due to enhanced inter-colloidal collision at higher concentrations, leading to increased detachment of colloids, weakly attached (i.e. at secondary energy minima) to the collector grains. Linear increase in inter-colloidal collision frequency (F_c) with increase in colloidal number concentration (n) is expressed as [19]:

$$F_C = n\pi D^2 v_r \quad (1)$$

Where D is the diameter of the particles and v_r is velocity of one particle relative to other particles.

Increasing the injection concentration of nanobubbles (gas containing bubbles used for water treatment, soil remediation of organic chemicals etc.) for enhancing nanobubbles-deposited latex colloidal collision probability and therefore removal of attached latex colloids on porous media has been suggested by Sugimoto, Hamamoto and Nishimura, [76].

Aqueous phase colloid-solid phase colloid collisions had been suggested to be a probable mechanism for reversal of nanoscale arsenic thiosulphate aggregation and detachment from porous media [93]. A similar mechanism was proposed by Sun et al., [79] to remove zinc oxide (ZnO) nanoparticles from soil particles deposited at weak secondary energy minima with an energy barrier of only $-1.2k_BT$ at pH 8.5. However, extended release of deposited ZnO nanoparticles under acidic conditions was attributed to dissolution of the particles due to increasing ZnO solubility with decreasing pH [34]. The effluent concentration of ZnO nanoparticles showed an increase with increasing injection concentrations, with no obvious trend of attachment and detachment coefficients, from 82 to 430 mg/L in soil system. Depending on the depth of existing energy barrier between the particles, colloids were reported to aggregate due to higher collision frequency with increasing injection concentration as well, resulting in higher deposition [23]. Most of the concentration ranges (Fig. 1.1) investigated are within only 2–3 order of magnitudes with little or no inter-study overlap. Though this work (Fig. 1.1) provides an overview of the parameters (k_{att}, k_{det}, α, η_0) and processes (e.g. blocking, aggregation, knocking off) responsible for colloidal retention and transport as a function of C_0, there is a gap in research covering deposition kinetics as a function of a wide a range of C_0.

The choice of the colloidal particles for this study was directed by the advantage of SiDNASi being environmentally nontoxic, uniquely sequenced, low detection limit and no background noise in natural environment [41,51,52]. Silica encapsulation is advantageous for its capability of acting as a physical barrier between delicate DNA molecules and chemical (e.g. metal ions) and physical (e.g. pH, temperature and ionizing radiation) environmental stresses, high chemical and thermal stability, nontoxicity, ability to be synthesized and dissolute at room temperature and chemical compatibility with nucleic acid analysis [53,56,60]. Use of these particles is also gaining increasing attention as a potential hydrological tag for investigating subsurface [4,51,54,66], surface [27,28,45,80] and glacial [20] hydrological systems. The concentration range was selected based on its relevance in natural subsurface systems.

The objective of this study was to investigate the quantitative effect of a broad spectrum (7 orders of magnitude) of SiDNASi injection concentrations on colloidal transport and retention parameters through saturated sand columns. We hypothesized that if removal of colloids associated with collector grains would depend on colloidal injection concentration (C_0), then in systems free of clogging, site saturation and with constant water quality, the single collector removal efficiency (η) would remain constant as a function of C_0.

2. Materials and methods

2.1. Silica encapsulated DNA colloidal particles (SiDNASi)

4 mg/ml ($\sim 4 \times 10^{10}$ particles/ml) SiDNASi dispersions (Silica encapsulated 80 bp dsDNA) were obtained from ETH, Zurich, prepared at Functional Materials Laboratory at the Institute of Chemical and Bioengineering, ETH, Zurich, Switzerland, produced using the protocol detailed in Mikutis et al. [51]. The particle number concentration was calculated by dividing the W/V concentration (4 mg/ml) of stock suspension by approximated particle weight (obtained from W/V particle concentration and particle number concentration information at the manufacturing lab). A calibration curve was prepared (qPCR) from the stock suspension to determine the DNA concentration and SiDNASi/ml concentrations used for injection experiments. Zeta potential (ζ) and hydrodynamic diameter ($Ø_h$) (Malvern Panalytical Zetasizer Nano-Zs ZEN 3600, the Netherlands) were measured with a concentration of $\approx 4 \times 10^7 - 4 \times 10^8$ particles/ml dispersed in 5 mM phosphate buffer using dynamic light scattering (DLS) method (173^0 backscattering). 5 mM phosphate buffer prepared using $0.77 gL^{-1}$ of $Na_2HPO_4 \bullet 7\ H_20$ (0.0029 M) (EMSURE®, Merck KgaA, Germany) and $0.29 gL^{-1}$ of $NaH_2PO_4 \bullet H_20$ (0.0021 M) (J.T.Baker, Spain) dissolved in demineralized water. The pH was adjusted to 7.0–7.1 using 100 mM NaOH (J.T. Baker, Poland).

2.2. Column preparation

To remove surface associated metal oxides (e.g. K^+,Ca^{2+},Mg^{2+},Fe^{3+}) and chemical nonidealities [31,46,90], 355–425 μm diameter grain size quartz sand (Sibelco, Soignes, Belgium), with a median diameter of 400 μm, was acid washed by soaking in 4 N 65 % nitric acid (HNO_3) for 2 h. The acid-soaked sand was further washed with demineralized water till an electric conductivity of $< 2\mu S/cm$ was achieved. The wet sand was then dried at 105^0 C in drying oven (TERMAKS, series TS8000, Germany).

The acid washed sand was packed in duplicate Polyvinyl chloride columns (15 cm long and ID 2.1 cm; Milder B.V., Rotterdam, the Netherlands) in 1-cm increments under constant vibration in order to avoid air entrapment and layering. The sand volume was treated with carbon-di-oxide ($CO_{2(g)}$) in a closed lid container to eliminate air pockets in the saturated column since $CO_{2(g)}$ has a higher solubility in water than air. Injection suspension was injected at the bottom of each column using a peristaltic pump for suspension injection (WATSON MARLOW 101 U/R and BT100–2 J) and samples were collected using an automatic fraction collector (OMNICOLL Fraction Collector, Lambda Laboratory Instruments) from the top of the columns (Fig. 2.1). Prior to each experiment, the columns were equilibrated with at least 10–12 pore volumes of 5 mM phosphate buffer. The porosity (ε) of the sand packed columns were measured gravimetrically using:

$$\varepsilon = \frac{W_{SS} - W_{DS}}{v_c} \quad (2)$$

Where W_{DS} is dry sand weight [gram], W_{SS} is saturated sand weight [gram], v_c is the total volume of the column [cm^3]. Under completely saturated conditions, the difference between W_{DS} and W_{SS} was considered for determining total void volume [26].

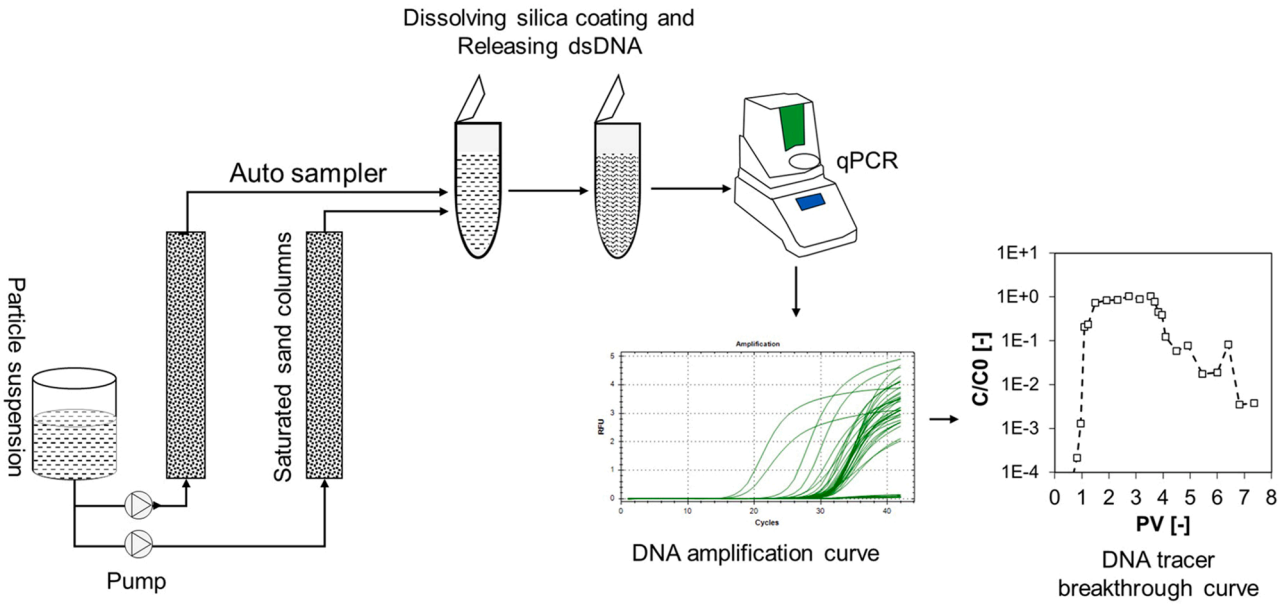

Fig. 2.1. Schematic set up of the column experiments. Sand packed (Ø 355–425 μm) PVC columns (l=15 cm; ID=2.1 cm) in duplicate were fed with SiDNASi suspension of different injection concentrations using a peristaltic pump (bottom-top direction).

2.3. Column injection experiments

Following the equilibration of the columns with 5 mM phosphate buffer, 66–70 ml (ca. 3 pore volumes) of seven SiDNASi injection concentrations ranging from 8.72×10^2 to 6.6×10^8 particles/ml (Table 2.1) were injected at a flow rate of 0.3 ml/min. Then, 4–5 PVs of particle free solution was injected with subsequent injection of demineralized water (low IS solution) in order to obtain an insight into the type of colloidal-collector kinetic interaction and reversibility of colloid retention process. An overview of the experimental episodes has been summarized below (Table 2.1). The pH of the column influent and effluent were monitored to be stable between 7 and 7.2. Prior to particle injection, conservative salt tracer transport tests were conducted with 3 pore volumes (PVs) of NaCl to check the column packing as well as obtaining ε and D. Particle injection suspensions were well mixed using a magnetic stirrer throughout the injection period and 3–5 samples were collected to determine the stability of injection concentration throughout the injection duration. Samples were collected every 5 min in 15-ml polypropylene tubes. NaCl injection experiment samples were analysed using an electric conductivity sensor (WTW-Portable conductivity meter ProfiLine Cond 3310, Germany) and SiDNASi samples were quantified using quantitative polymerase chain reaction (qPCR) as described in the next section.

2.4. Sample analysis

20 μL sample was mixed with 1 μL of buffered Oxide Etch (BOE) for dissolving silica and releasing DNA in suspension, followed by addition of 100 μL of TRIS-HCl to stabilize pH. 5 μL of this suspension was mixed with 1 μL of sequence specific, 17 base pair long reverse and forward primers (40–45 % GC content) obtained from Biolegio (Biolegio B.V, Nijmegen, the Netherlands) and 13 μL of KAPA SYBR FAST qPCR enzyme master mix (KAPA SYBR® FAST, KK4601 07959389001, South Africa). BOE comprises equal proportions of Ammonium hydrogen Difluoride (NH_4FHF) [51] (Sigma Life Sciences, the Netherlands) and Ammonium Fluoride (NH_4F) (J.T.Baker®, Holland). Diethyl-pyrocarbonate (DEPC)-treated and sterile filtered water was used for sample preparation. All mixing was done using a QIAgility high-precision automated PCR set up (QIAgility System HEPA/UV, Cat No. /ID: 9001532).

The DNA amplification protocol in MiniOpticonTM detector Real-Time PCR system (Bio-Rad laboratories, USA and Singapore) started with one-time sample treatment at 95 °C for 280 s followed by 41 cycles of 90 °C for 14 s, 58 °C for 27 s and 72 °C for 25 s. The outputs, obtained as quantification cycle (Cq) values, were converted to particle concentrations using a standard dilution curve. A positive control and no template controls (NTCs) were included in sample series analysis for quality control. All positive controls were similar and the negative controls were sufficiently high (Ct>30 amplification cycles) to warrant for the detection specificity of the DNA sequences at low concentrations and contamination free analysis.

2.5. Breakthrough curve analysis and 1D modeling

One-dimensional advective transport, longitudinal dispersivity, first-order kinetic attachment and detachment are the processes considered

Table 2.1
Column injection experiment concentrations and episodes.

Particles/ml	Porosity [-]	Dispersivity (Std err.) [cm]	Episode 1	Episode 2	Episode 3	Episode 4
6.6×10^8 4.7×10^7 3.2×10^6 4.2×10^5 4.8×10^4 3.7×10^3 8.7×10^2	≈ 0.40	6.24×10^{-2} (1.9×10^{-3})	Equilibrate with phosphate buffer (5 mM) for 10–12 PVs	2.5–3 PV particle suspension	4–5 PVs of particle free suspension	5–6 PVs of lower ionic strength solution (demineralized water)

to be major for our experimental conditions. In this study, upon comparing the goodness of fit for the curve fitting and Akaike Information criteria for one-site and two-site attachment/detachment model, one-site attachment/detachment model (Eq. 3) was used for experimental curve fitting and parameter optimization. The overall transport equation [75] used was as follows:

$$\frac{\partial \theta c}{\partial t} + \theta k_{att} \Psi c - k_{det} \rho s = \frac{\partial}{\partial x}\left(\theta D \frac{\partial c}{\partial x}\right) - \frac{\partial qc}{\partial x} \quad (3)$$

Where c is the colloid concentration in liquid phase [particles/ml], t is transport time [min], k_{att}, k_{det} are the first order kinetic attachment and detachment rate coefficient, respectively [min^{-1}], $\Psi = (1\text{-}s/s_{max})$ is the dynamic blocking function [-] applied for the highest injection concentration, s is kinetically attached particle on solid phase [number of particles/g of sand], s_{max} is the maximum solid phase concentration [number of particles/g of sand], θ is the volumetric water content [-], q is the Darcy flux [cm/min], D is the longitudinal dispersion coefficient [cm^2/min], and x is the spatial coordinate along the transport length [cm].

To consider the effect of blocking on k_{att} we used the product of Ψ and first order kinetic attachment rate coefficient, denoted by $k_{att}\Psi$, instead of using only first order k_{att}, where s tends to s_{max} [44]. The D and the estimations of $k_{att}\Psi$, k_{det}, s, and s_{max} were obtained by fitting experimental breakthrough curve with a one-site kinetic attachment-detachment, non-equilibrium particle transport model using an open source, widely used software package HYDRUS1D (v.4.17.014). Briefly, in HYDRUS 1D, a Galerkin-type linear finite element method was used to spatially discretize with finite difference methods for estimating the temporal derivatives. A Crank–Nicholson finite difference scheme was used for solving the advection–dispersion equation. Initially an objective function was defined [75], and further minimized using the Levenberg-Marquardt non-linear minimization method, a weighted least-squares approach based on Marquardt's maximum neighborhood method [50]. HYDRUS1D was chosen for parameter optimization and estimation since the model was open source, well documented and widely used.

D and ε were optimized by fitting salt tracer breakthrough curve to the solute transport code. Then ε was then compared with the gravimetric method.

The single collector contact efficiency ($\eta_{0,CFT}$), for calculating the single collector sticking efficiency (α), was determined by Tufenkji-Elimelech (TE) correlation equation [85] considering a Hamaker constant of 5×10^{20}J. The k_{att} and $\eta_{0,CFT,}$ obtained from Eq. 3 and TE correlation equation, respectively, were further used to compute α, using Eq. 4 [85]. However, in order to evaluate the effect of Ψ for the highest colloidal injection concentration, $k_{att}\Psi$ was used instead of k_{att}:

$$\alpha = \frac{4 k_{att} a_c}{3(1-\varepsilon) v_p \eta_{0,CFT}} \quad (4)$$

Where a_c is the collector sand grain radius [cm], v_p is the pore water velocity [cm/min].

In addition to kinetic attachment and detachment, as concluded by many researchers, colloidal mobility can also be influenced by filling up of maximum available attachment sites on the collector grains, by reaching a jamming limit [1,38]. In order to check whether attaining such limit is critical for any changes in k_{att} observed, the s and s_{max} obtained from the inverse fitting of experimental breakthrough curves were used to determine the fractional filling of favourable attachment sites or possibility of blocking. In order to determine whether a jamming limit had been reached for the injected concentrations, fractional collector surface coverage (θ) was determined as a ratio of collector surface covered by the maximum solid phase attached particles per gram of sand (s_{cov}) and maximum possible coverage of sand grains per gram of sand ($s_{max.cov}$). To calculate s_{cov}, the maximum particle number deposited s, was selected by comparing deposited particle number at different time steps throughout the experiment. This maximum was typically found to be at the immediate end of a loading phase. $s_{max.cov}$ was estimated by multiplying the total surface area of spherical collector grain per gram of sand and maximum surface coverage (θ_∞) possible for sphere on sphere deposition, given by Adamczyk et al. [1]:

$$\theta_\infty = 0.547\left(1 + \frac{a_c}{a_p}\right)^2 \quad (5)$$

2.6. DLVO interactions

DLVO interaction energy profiles based on the equation given by Loveland et al., [47] between colloid-colloid and colloid-collector grains were calculated in order to determine the strength of the interactions in terms of depth of secondary minima ($\Phi_{sec.min}$) and primary energy maxima ($\Phi_{pri.max}$) and therefore possibility of colloidal aggregation or deposition on collector grains (see eg S1 for the equation and Fig S1 for the DLVO profile).

3. Results

3.1. SiDNASi characterization

The hydrodynamic diameter and zeta potential (ζ) were found to be 280–300 nm and − 47.2 ± 7.6 mV at pH 7–7.1 and 23° C, respectively. The ζ was well above the accepted value (≥30 mV for electrostatic and ≥20 mV for steric stabilization) for which the inter-particle repulsion is large enough to overcome the van der Waal forces, therefore remaining well dispersed in the aqueous phase rendering the colloidal suspension stable [2,8,55]. Since the ζ measurement was restricted to a concentration of ≈ 4×10^7 to 4×10^8 particles/ml due to instrument limitation, evaluating the particle concentration dependent change in $Ø_h$ and ζ due to phosphate buffer was not feasible. However, such changes were not expected since the phosphate ions were in well excess (3×10^{21}ions/ml) as compared to the particle number concentration (phosphate ions: particles ratio of ≈7×10^{12}).

3.2. NaCl breakthrough

The effective porosity (ε) determined gravimetrically (≈0.39–0.40) and from iteration based HYDRUS1D code (0.42) were in good agreement with each other. The longitudinal dispersivity (D) was estimated to be ≈ $6.24 \times 10^{-2} \pm 1.9 \times 10^{-3}$ cm for the duplicate columns. Symmetrical salt tracer breakthrough curves indicated the absence of dual porosity and sink pockets inside the columns. These values were further used for curve fitting of SiDNASi breakthrough curves considering that the dispersion behaviour for the conservative tracer and the colloidal particles are comparable since the peclet number of the experimental conditions were high (Pe >1) indicating an advection dominated transport. The coefficient of determination (R^2) between observed and fitted salt breakthrough curves was 0.99 ± 0.002.

3.3. Particle breakthrough curve from saturated sand columns

Breakthrough curve behaviour – The maximum effluent colloidal particle concentrations (C_{max}/C_0) (Fig. 3.1) differed within one order of magnitude between experiments and increased with increasing particle injection concentration(C_0), apparently due to less retention of particles at a higher injection concentration. There was no delayed or early breakthrough observed for any of the concentrations relative to the conservative NaCl tracer. This agreed with the assessment that there was no preferential flow domain or retardation of the SiDNASi. The plateau phase for the SiDNASi breakthrough curves were attained between 1.2 and 1.5 pore volumes of injection and remained till 3–4 pore volume of injection following similar trend of salt injection solution, however, the declining limb showed significant tailing as compared to a sharp decline

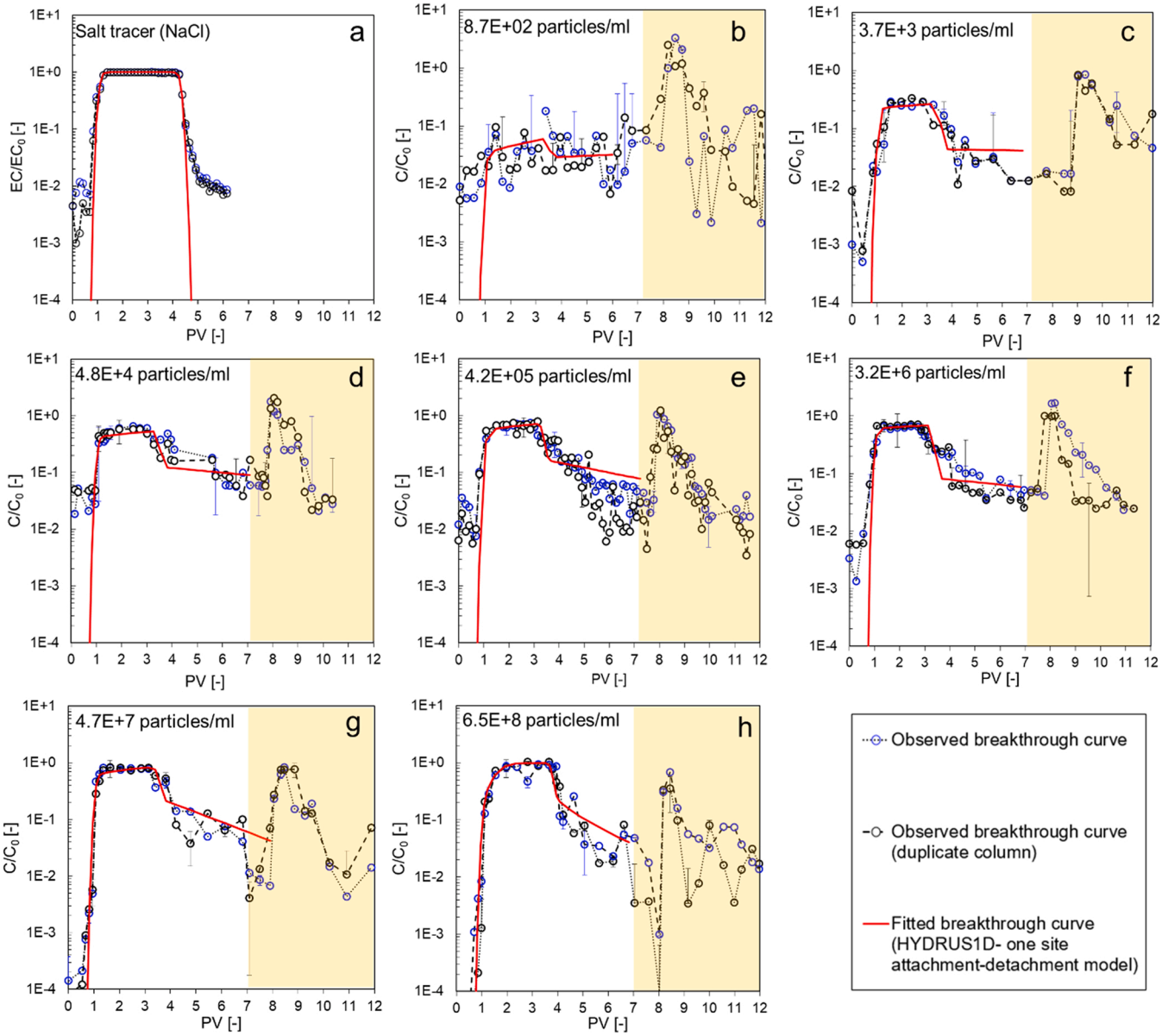

Fig. 3.1. Relative SiDNASi particle concentrations observed in column effluent in duplicate. Figs. a and b-h represent the breakthrough curves for conservative tracer (NaCl) and different SiDNASi injection concentrations ranging from 8.7×10^{2} to 6.5×10^{8} particles/ml with one site kinetic attachment-detachment model fitted breakthrough curve (solid red line), respectively. The white blocks denote the injection of SiDNASi particle suspension followed by background solution injection (episode 2 and 3) and the yellow blocks denote the demineralized injection episode (episode 4).

for NaCl injection solution. Prior to demineralized water (low IS solution) injection, similar to maximum effluent colloidal particle concentration, mass recovery also showed pronounced differences among concentrations. Mass recoveries were estimated to be 10 %, 33 %, 65 %, 67 %, 62 %, 74 %, and 83 % with increasing injection concentration, respectively. The complete set of breakthrough curves in Fig. 3.1 showed that injection of lower ionic strength water removed most of the retained particles, supported by the total mass recoveries of nearly 100 %. Regression analysis between the observed and model estimated data demonstrated $>$ 85 % agreement for all concentrations, but 8.7×10^{2} particles/ml (Table 3.1. Low injection concentration as well as high colloidal retention led to effluent particle concentration near to detection limit, in turn, higher measurement errors.

3.4. First order kinetic attachment (k_{att}) and detachment rate (k_{det})

At first, we tried both one-site and two-site attachment/detachment. However, a comparison between one-site and two-site revealed the two-site model was not better than the one-site in terms of goodness of curve fitting and Akaike Information Criteria (data not shown). Therefore, we chose to further use optimized parameters from the one-site model. The k_{att} ranged between 4.4×10^{-2} and 1.7×10^{-3} min^{-1} (Fig. 3.2, Table 3.1, log-linearly decreasing within one order of magnitude with increasing injection particle concentration. The kinetic attachment rate for the highest SiDNASi injection concentration, is considered to be a product of k_{att} and blocking function since $\Psi < 0.1$. In contrast, the k_{det} increased with increasing injection concentration from 7.4×10^{-4} to $9.8\times10^{-3}min^{-1}$ (Table 3.1, combinedly indicating higher relative retention with lower injection particle concentration. The estimation errors at 95 % confidence interval ranging within one order of magnitude of the estimated values indicate high and comparable accuracies of the estimated values among different injection concentrations.

Table 3.1
SiDNASi injection concentration dependent k_{att} and k_{det} [min^{-1}] obtained from one site attachment-detachment model curve fitting, s_{max} and s [Particles/g of sand] denotes maximum solid phase and maximum number of attached SiDNASi particles at the end of loading phase, respectively. Calculation of $\eta_{0,exp}$ considers $\alpha_{max.exp}$= 9.42×10^{-2} [-].

C_0 [Particles/ml]	HYDRUS1D				
	k_{att} (Std error) [min^{-1}]	**K_{det} (Std error) [min^{-1}]**	**R^2 [-]**	**s_{max} (Std error) [particles/g of sand]**	**s [particles/g of sand]**
6.6×10^{8}	‡1.7×10^{-3} (3.6×10^{-4})	9.8×10^{-3} (3.4×10^{-3})	0.92	6.5×10^{7} (1.1×10^{7})	5.9×10^{7}
4.7×10^{7}	6.2×10^{-3} (8.5×10^{-4})	6.9×10^{-3} (1.9×10^{-3})	0.90	3.9×10^{12} (4.8×10^{-17})	4.7×10^{6}
3.2×10^{6}	6.5×10^{-3} (3.5×10^{-4})	1.8×10^{-3} (5.6×10^{-4})	0.88	4.3×10^{12} (4.9×10^{-17})	4.2×10^{5}
4.2×10^{5}	7.5×10^{-3} (4.8×10^{-4})	3.8×10^{-3} (5.2×10^{-4})	0.87	3.1×10^{12} (3.3×10^{-17})	5.6×10^{4}
4.8×10^{4}	1.1×10^{-2} (6.1×10^{-4})	2.1×10^{-3} (2.7×10^{-4})	0.80	7.3×10^{10} (5.5×10^{-17})	2.9×10^{4}
3.7×10^{3}	1.8×10^{-2} (1.3×10^{-3})	7.4×10^{-4} (1.9×10^{-4})	0.83	4.8×10^{12} (6.8×10^{-17})	1.3×10^{3}
8.7×10^{2}	4.4×10^{-2} (2.9×10^{-3})	1.3×10^{-3} (3.4×10^{-4})	0.17	3.9×10^{11} (1.4×10^{-16})	6.5×10^{2}

‡First order kinetic attachment rate for the highest SiDNASi injection concentration is $k_{att}\Psi$ (attachment rate * blocking function)

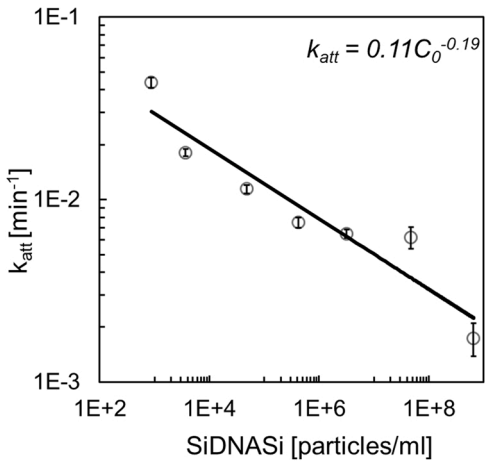

Fig. 3.2. Log-linear correlation of first order k_{att} [min^{-1}] with SiDNASi injection concentration. The kinetic attachment rate corresponding to the highest SiDNASi injection concentration is $k_{att}\Psi$ (attachment rate * blocking function).

3.5. Blocking function (Ψ) and fractional surface coverage (θ)

The maximum surface coverage (s_{max}) was found to be 6.5×10^{7} particles/g of sand, (Table 3.1. The surface coverages (s) ranged from 6.5×10^{2} to 5.9×10^{7}, increased with increasing SiDNASi injection concentration. The blocking function (Ψ) estimated from s and s_{max}, being $s << s_{max}$ and therefore $\Psi\rightarrow1$, indicated that time-dependent retention of SiDNASi particles due to filing up of favourable particle retention sites did not play a significant role in the particle retention. However, for the highest injection concentration (6.6Ex10^{8} particles/ml), s was 0.91 s_{max}, indicating maximum colloidal retention sites to be filled up slightly over 90 % of the total available retention sites. In view of SiDNASi size (a_c=2.8×10^{-5}cm) and collector (a_p =4×10^{-2}cm) radius, the maximum fraction of surface coverage (θ_∞) of the spherical collector grain by SiDNASi particle possible was 5.47×10^{-2}. The fractional surface coverage (θ), as a ratio of collector surface coverage by SiDNASi particles (s_{cov}) and maximum possible collector grain surface coverage ($s_{max.cov}$), ranged between 1.7×10^{-8} to 6.2×10^{-2}, with increasing injection concentration.

3.6. Sticking (α), single collector contact (η_0) and removal efficiency (η)

The sticking efficiency (α) determined using TE correlation equation was found to be ranging between 2.16×10^{-1} and 8.58×10^{-3}, and decreased with increasing injection concentration. The single collector contact efficiency (η_0) was 4.52×10^{-2} [-], using the TE correlation equation.

3.7. DLVO calculation

The depth of secondary energy minima ($\Phi_{sec.min}$) for inter-colloidal interaction (Fig S1) was − 0.05k_BT. The energy barrier ($\Phi_{pri.max}$) for irreversible deposition for both the scenarios was at least one order of magnitude higher than 300k_BT, indicating that deposition in the primary minima was unlikely and deposition in the secondary minima energy well was the primary mechanism of colloidal retention.

4. Discussion

With an increasing colloidal injection concentration of SiDNASi under saturated conditions, the maximum effluent concentration (C_{max}/C_0) increased, which was in agreement with Wang et al. [87], Bradford and Bettahar [9], Bradford et al. [10] and Vitorge et al. [86]. The first order k_{att} decreased log linearly with increasing injection concentration, which was consistent with Wang et al., [87], though the underlying mechanism had been attributed to blocking by the authors. However, for the highest injection concentration blocking function was estimated to be < 0.1, indicating the k_{att} could be influenced by gradual filling up of the available colloidal retention sites. The correlation equation between k_{att} and C_0 indicated that at a given SiDNASi injection concentration, k_{att} was inversely dependent on the fifth root of injection concentration. On the other hand, the k_{det} declined with increasing injection concentration leading to reduced retention at higher injection concentrations.

The concentration dependence of first order k_{att}, k_{det} and overall colloidal retention under consistent physico-chemical experiment conditions could have been arisen either due to changes in α or the η_0. The α estimated applying the k_{att} coefficient obtained from the curve fitting method in Eq. 4 indicated an inverse relation with the SiDNASi injection concentration, considering that η_0 is constant. However, since α was dependent on the injection solution chemistry and collector surface properties, it is constant under current experimental conditions. Therefore, alternatively we considered α to be constant and propose that the concentration dependent variation of colloidal retention is possibly due to the effect of injection concentration on the single collector collision efficiency (η_0). Considering a value of 9.42×10^{-2} [-] for α_{max}, corresponding to the injection concentration 3.7×10^{3} particle/ml, both the η_0 and η showed a log linear inverse dependence on the injection SiDNASi particle injection concentration, decreasing with increasing injection concentration. The constant value of α represented maximum attachment efficiency observed in our experimental condition assuming the intercolloidal interaction was relatively negligible (e.g. pH ~7.0, IS 5 mM, Temperature 23^0 C). Injection concentration 3.7×10^{3} was preferred over 8.7×10^{2} particles/ml, since the lowest concentration did not show a well-formed breakthrough curve, effluent concentrations were near detection limit with a low coefficient of determination (R^2 =0.17) for curve fitting, indicating low confidence of the parameters estimated.

According to TE correlation equation, η_0 is colloidal injection concentration independent considering that the injection concentration does not significantly alter the colloid size due to aggregation, porosity or approach fluid velocity [85]. Since different underlying attachment and detachment mechanisms could not be distinguished through the numerical model, we propose to attribute the effect of increasing SiDNASi injection concentration as overall log linear reduction in η. More

specifically, η log linearly reduced from 9.7×10^{-3} to 3.9×10^{-4} as a function of increasing SiDNASi injection concentration. However, a systematic porous scale observation needs to be conducted to determine the underlying mechanism of such concentration dependent changes in colloidal removal efficiency.

Since physicochemical conditions for all the column experiments were consistent, site saturation as well as pore clogging or straining were not relevant (particle to collector grain ratio ranged from 7.05×10^{-4} to 8.45×10^{-4} in our experiments, which was more than one order of magnitude lower than the threshold value [59]), colloidal deposition was either weak, secondary energy minima dominated, or due to nanoscale surface charge heterogeneities. Increasing k_{det} and enhanced mobility of SiDNASi with increasing concentration could be attributed to electrostatic double layer repulson between the aqueous phase and deposited SiDNASi [39,42] and by developing a shadow zone downgradient of the deposited particles restricting the probability of subsequent colloidal deposition [40,69]. Release of weakly attached SiDNASi (deposited in secondary energy minimum or nanoscale surface asperities) could also be attributed to enhanced electrostatic colloid-collector repulsion or charge reversal of surface charge heterogeneities due to adsorption of phosphate onto both collector grains and colloid particles [16,88]. Another possible explanation of the concentration dependent changes in k_{att} and η could be colloidal re-entrainment due to aqueous phase-solid phase inter-colloidal collision. Intercolloidal collision, being a linear function of particle number density, as in $F_C=n\pi D^2 v_r$ [19], increased with increasing SiDNASi injection concentration [74,77,84]. Increase in the aqueous phase-solid phase colloidal collision frequency with increasing injection concentration resulted in a higher percentage of weakly attached SiDNASi removal from collector grains at higher concentration than in subsequent lower concentrations, a mechanism hypothesized by Bradford et al., [10] for polystyrene latex microparticles. Increase in 'knocking off' and therefore removal of particles from the collector grain was also observed in the increasing effluent mass recovery with increasing injection concentration. The concept of increased colloid-colloid collision leading to removal of weakly deposited colloids has also been mentioned for zinc oxide nanoparticles [78] under alkaline conditions from soil particles or removal of latex colloids [76]. Though inter-colloidal collisions have been reported to cause colloidal aggregation and therefore higher deposition [23], we think SiDNASi aggregation was unlikely to occur under current environmental conditions: for higher SiDNASi concentrations than the ones we used, Tang et al., [80] reported a constant hydrodynamic diameter in 5 mM phosphate buffer in both quiescent (4 h) and mixing (3 h) conditions. Furthermore, if aggregation as a function of increasing SiDNASi concentrations would have occurred, then this would have likely caused more retention; instead we observed less retention with increasing injection concentration. A more detailed pore scale investigation would be required to distinguish between different attachment and detachment mechanisms contributing to the mobility of SiDNASi and the effect of injection concentration.

Under current experiment conditions, the attachment-detachment model demonstrated that the attachment theory well explained observed SiDNASi breakthrough behaviour. However, the numerical model cannot distinguish between attachment and retention due to straining [14,65].

In addition, the correlation between $k_{att,}$ k_{det} and C_0 might be specific to the up-flow direction as used in our work since flow direction has been reported to significantly influence colloidal deposition [6,18]. Surface roughness had comparatively limited influence on particle deposition in up-flow orientation. Therefore, while comparing k_{att} and k_{det} of different or even same colloids in different studies, the flow direction should be carefully considered since gravity can have significant effect on the retention mechanism. Not considering flow direction can also have implications while comparing experimental data within the colloid filtration theory (CFT) framework, developed for downward flow direction Chrysikopoulos and Syngouna [18].

5. Conclusion

- The current work illustrates a systematic investigation of the influence of injection concentration of silica encapsulated silica core DNA colloidal microparticle (SiDNASi) on their migration characteristics and interaction with one dimensional saturate porous media, under unfavourable deposition conditions
- The SiDNASi mass recovery, prior to the injection of low ionic strength water (DI water), increased with increasing injection concentration
- Colloidal attachment onto collector grain could be explained well using a one-dimension model considering first order k_{att} and k_{det}. The k_{att} and k_{det} respectively decreased and increased with increasing injection SiDNASi concentration.
- The k_{att} reduced with increasing SiDNASi injection concentration, indicating an overall decrease in single collector removal efficiency. The increased SiDNASi mobility with increased injection concentration could be due to electrostatic repulsion between aqueous phase and deposited colloids, enhanced colloid-collector electrostatic repulsion due to phosphate adsorption and/or increase in aqueous phase-solid phase colloidal collisions leading to removal of deposited particles.
- The connotations of these findings are two-fold. Firstly, the significance of understanding the colloidal retention trend and probable processes as a function of injection SiDNASi concentration, and, secondly, colloidal retention dynamics in studies using injection concentrations, differing in orders of magnitude, should not be compared or generalized without considering the concentration effect on k_{att}.
- The reduction in SiDNASi retention and η as a function of the wide range of increasing injection concentration used in this study, would be applicable to colloidal mobility in any porous media system devoid of colloid aggregation and pore clogging where an unfavourable condition for colloid deposition persists.
- The primary limitation of this approach could be that the numerical relationship between single collector removal efficiency and injection concentration might be experimental system specific and might alter depending on physicochemical parameters such as flow velocity, ionic strength, flow orientation etc. Therefore, possibility of proposing a generalized numerical correlation is limited

CRediT authorship contribution statement

Swagatam Chakraborty: Conceptualization, Methodology, Formal analysis, Investigation, Writing – original draft; **Jan Willem Foppen:** Conceptualization, Writing – review & editing, Resources, Supervision; **Jack F. Schijven:** Conceptualization, Writing – review & editing, Resources, Supervision.

Declaration of Competing Interest

The authors declare that they have no known competing financial interests or personal relationships that could have appeared to influence the work reported in this paper.

Data Availability

Data will be made available on request.

Acknowledgement

This research had been financially supported by The Dutch Research Council (NWO), TTW grant 14514. We would like to extent our gratitude towards Institute of Chemical and Bioengineering, ETH, Zurich, Switzerland for the kind contribution with the SiDNASi particles.

Appendix A. Supporting information

Supplementary data associated with this article can be found in the online version at doi:10.1016/j.colsurfa.2022.129625.

References

[1] Z. Adamczyk, M. Nattich-Rak, M. Sadowska, A. Michna, K. Szczepaniak, Mechanisms of nanoparticle and bioparticle deposition–Kinetic aspects, Colloids Surf. A: Physicochem. Eng. Asp. 439 (2013) 3–22.
[2] J. Alves Júnior, J. Baldo, The behavior of zeta potential of silica suspensions. new journal of glass and ceramics 04 (2014) 29–37.
[3] M. Amme, L. Aldave de las Heras, M. Betti, H. Lang, M. Stöckl, Effects of colloidal and dissolved silica on the dissolution of UO2 nuclear fuel in groundwater leaching tests, J. Radioanal. Nucl. Chem. 261 (2) (2004) 327–336.
[4] L. Aquilanti, F. Clementi, T. Nanni, S. Palpacelli, A. Tazioli, P.M. Vivalda, DNA and fluorescein tracer tests to study the recharge, groundwater flowpath and hydraulic contact of aquifers in the Umbria-Marche limestone ridge (central Apennines, Italy), Environ. Earth Sci. 75 (7) (2016) 626.
[5] H. Bai, N. Cochet, A. Drelich, A. Pauss, E. Lamy, Comparison of transport between two bacteria in saturated porous media with distinct pore size distribution, Rsc Adv. 6 (18) (2016) 14602–14614.
[6] H.A. Basha, P.J. Culligan, Modeling particle transport in downward and upward flows, Water Resour. Res. 46 (2010) 7.
[7] A. Beryani, M.R.A. Moghaddam, T. Tosco, C. Bianco, S.M. Hosseini, E. Kowsari, R. Sethi, Key factors affecting graphene oxide transport in saturated porous media, Sci. Total Environ. 698 (2020), 134224.
[8] S. Bhattacharjee, DLS and zeta potential–what they are and what they are not? J. Control. Release 235 (2016) 337–351.
[9] S.A. Bradford, M. Bettahar, Concentration dependent transport of colloids in saturated porous media, J. Contam. Hydrol. 82 (1–2) (2006) 99–117.
[10] S.A. Bradford, H.N. Kim, B.Z. Haznedaroglu, S. Torkzaban, S.L. Walker, Coupled factors influencing concentration-dependent colloid transport and retention in saturated porous media, Environ. Sci. Technol. 43 (18) (2009) 6996–7002.
[11] S.A. Bradford, J. Simunek, S.L. Walker, Transport and straining of E. coli O157: H7 in saturated porous media, Water Resour. Res. 42 (2006) 12.
[12] S.A. Bradford, J. Simunek, M. Bettahar, M.T. Van Genuchten, S.R. Yates, Modeling colloid attachment, straining, and exclusion in saturated porous media, Environ. Sci. Technol. 37 (10) (2003) 2242–2250.
[13] S.A. Bradford, S. Torkzaban, S.L. Walker, Coupling of physical and chemical mechanisms of colloid straining in saturated porous media, Water Res. 41 (13) (2007) 3012–3024.
[14] S.A. Bradford, S.R. Yates, M. Bettahar, J. Simunek, Physical factors affecting the transport and fate of colloids in saturated porous media, Water Resour. Res. 38 (12) (2002) 63.1–63.12.
[15] G. Chen, S.L. Walker, Fecal indicator bacteria transport and deposition in saturated and unsaturated porous media, Environ. Sci. Technol. 46 (16) (2012) 8782–8790.
[16] M. Chen, N. Xu, X. Cao, K. Zhou, Z. Chen, Y. Wang, C. Liu, Facilitated transport of anatase titanium dioxides nanoparticles in the presence of phosphate in saturated sands, J. Colloid Interface Sci. 451 (2015) 134–143.
[17] I. Chowdhury, Y. Hong, R.J. Honda, S.L. Walker, Mechanisms of TiO_2 nanoparticle transport in porous media: Role of solution chemistry, nanoparticle concentration, and flowrate, J. Colloid Interface Sci. 360 (2) (2011) 548–555.
[18] C.V. Chrysikopoulos, V.I. Syngouna, Effect of gravity on colloid transport through water-saturated columns packed with glass beads: modeling and experiments, Environ. Sci. Technol. 48 (12) (2014) 6805–6813.
[19] Crowe, C., Sommerfeld, M. & Tsuji, Y. , 1998). Multiphase Flows with droplets and particles: Ż.
[20] H.E. Dahlke, A.G. Williamson, C. Georgakakos, S. Leung, A.N. Sharma, S.W. Lyon, M.T. Walter, Using concurrent DNA tracer injections to infer glacial flow pathways, Hydrol. Process. 29 (25) (2015) 5257–5274.
[21] M. Elimelech, Predicting collision efficiencies of colloidal particles in porous media, Water Res. 26 (1) (1992) 1–8.
[22] M. Elimelech, M. Nagai, C.H. Ko, J.N. Ryan, Relative insignificance of mineral grain zeta potential to colloid transport in geochemically heterogeneous porous media, Environ. Sci. Technol. 34 (11) (2000) 2143–2148.
[23] D.A. Ersenkal, A. Ziylan, N.H. Ince, H.Y. Acar, M. Demirer, N.K. Copty, Impact of dilution on the transport of poly (acrylic acid) supported magnetite nanoparticles in porous media, J. Contam. Hydrol. 126 (3–4) (2011) 248–257.
[24] A.R. Esfahani, A.F. Firouzi, G. Sayyad, A.R. Kiasat, Transport and retention of polymer-stabilized zero-valent iron nanoparticles in saturated porous media: Effects of initial particle concentration and ionic strength, J. Ind. Eng. Chem. 20 (5) (2014) 2671–2679.
[25] M. Fazeli Sangani, G. Owens, A. Fotovat, Transport of engineered nanoparticles in soils and aquifers, Environ. Rev. 27 (1) (2019) 43–70.
[26] L.E. Flint, A.L. Flint, 2.3 Porosity. methods of soil, Anal.: Part 4 Phys. Methods 5 (2002) 241–254.
[27] J.W. Foppen, C. Orup, R. Adell, V. Poulalion, S. Uhlenbrook, Using multiple artificial DNA tracers in hydrology, Hydrol. Process. 25 (19) (2011) 3101–3106.
[28] J.W. Foppen, J. Seopa, N. Bakobie, T. Bogaard, Development of a methodology for the application of synthetic DNA in stream tracer injection experiments, Water Resour. Res. 49 (9) (2013) 5369–5380.
[29] J.W. Foppen, M. van Herwerden, J. Schijven, Transport of Escherichia coli in saturated porous media: dual mode deposition and intra-population heterogeneity, Water Res. 41 (8) (2007) 1743–1753.
[30] G.J. Gentile, M.M.F. de Cortalezzi, Enhanced retention of bacteria by TiO2 nanoparticles in saturated porous media, J. Contam. Hydrol. 191 (2016) 66–75.
[31] I.G. Godinez, C.J. Darnault, Aggregation and transport of nano-TiO2 in saturated porous media: effects of pH, surfactants and flow velocity, Water Res. 45 (2) (2011) 839–851.
[32] M.J. Gross, O. Albinger, D.G. Jewett, B.E. Logan, R.C. Bales, R.G. Arnold, Measurement of bacterial collision efficiencies in porous media, Water Res. 29 (4) (1995) 1151–1158 (kim).
[33] M.W. Hahn, C.R. O'Melia, Deposition and reentrainment of Brownian particles in porous media under unfavorable chemical conditions: Some concepts and applications, Environ. Sci. Technol. 38 (1) (2004) 210–220.
[34] Y. Han, G. Hwang, D. Kim, S.A. Bradford, B. Lee, I. Eom, P.J. Kim, S.Q. Choi, H. Kim, Transport, retention, and long-term release behavior of ZnO nanoparticle aggregates in saturated quartz sand: Role of solution pH and biofilm coating, Water Res. 90 (2016) 247–257.
[35] B.Z. Haznedaroglu, H.N. Kim, S.A. Bradford, S.L. Walker, Relative transport behavior of Escherichia coli O157: H7 and Salmonella enterica serovar pullorum in packed bed column systems: influence of solution chemistry and cell concentration, Environ. Sci. Technol. 43 (6) (2009) 1838–1844.
[36] B.D. Honeyman, Colloidal culprits in contamination, Nature 397 (6714) (1999) 23–24.
[37] J. Hou, M. Zhang, P. Wang, C. Wang, L. Miao, Y. Xu, Z. Liu, Transport, retention, and long-term release behavior of polymer-coated silver nanoparticles in saturated quartz sand: the impact of natural organic matters and electrolyte, Environ. Pollut. 229 (2017) 49–59.
[38] Johnson, & Elimelech, Dynamics of colloid deposition in porous media: Blocking based on random sequential adsorption, Langmuir 11 (3) (1995) 801–812.
[39] P.R. Johnson, N. Sun, M. Elimelech, Colloid transport in geochemically heterogeneous porous media: modeling and measurements, Environ. Sci. Technol. 30 (11) (1996) 3284–3293.
[40] C.H. Ko, M. Elimelech, The "shadow effect" in colloid transport and deposition dynamics in granular porous media: measurements and mechanisms, Environ. Sci. Technol. 34 (17) (2000) 3681–3689.
[41] X.Z. Kong, C.A. Deuber, A. Kittilä, M. Somogyvári, G. Mikutis, P. Bayer, W.J. Stark, M.O. Saar, Tomographic reservoir imaging with DNA-labeled silica nanotracers: the first field validation, Environ. Sci. Technol. 52 (23) (2018) 13681–13689.
[42] F. Kuhnen, K. Barmettler, S. Bhattacharjee, M. Elimelech, R. Kretzschmar, Transport of iron oxide colloids in packed quartz sand media: monolayer and multilayer deposition, J. Colloid Interface Sci. 231 (1) (2000) 32–41.
[43] H.F. Lecoanet, M.R. Wiesner, Velocity effects on fullerene and oxide nanoparticle deposition in porous media, Environ. Sci. Technol. 38 (16) (2004) 4377–4382.
[44] Y. Li, Y. Wang, K.D. Pennell, L.M. Abriola, Investigation of the transport and deposition of fullerene (C60) nanoparticles in quartz sands under varying flow conditions, Environ. Sci. Technol. 42 (19) (2008) 7174–7180.
[45] R. Liao, P. Yang, W. Wu, D. Luo, D. Yang, A DNA tracer system for hydrological environment investigations, Environ. Sci. Technol. 52 (4) (2018) 1695–1703.
[46] Q. Liu, V. Lazouskaya, Q. He, Y. Jin, Effect of particle shape on colloid retention and release in saturated porous media, J. Environ. Qual. 39 (2) (2010) 500–508.
[47] J.P. Loveland, J.N. Ryan, G.L. Amy, R.W. Harvey, The reversibility of virus attachment to mineral surfaces. colloids and surfaces A: Physicochemical and engineering aspects 107 (1996) 205–221.
[49] N. Lu, C.F. Mason, Sorption-desorption behavior of strontium-85 onto montmorillonite and silica colloids, Appl. Geochem. 16 (14) (2001) 1653–1662.
[50] D.W. Marquardt, An algorithm for least-squares estimation of nonlinear parameters, J. Soc. Ind. Appl. Math. 11 (2) (1963) 431–441.
[51] G. Mikutis, C.A. Deuber, L. Schmid, A. Kittilä, N. Lobsiger, M. Puddu, W.J. Stark, Silica-encapsulated DNA-based tracers for aquifer characterization, Environ. Sci. Technol. 52 (21) (2018) 12142–12152.
[52] G. Mikutis, L. Schmid, W.J. Stark, R.N. Grass, Length-dependent DNA degradation kinetic model: decay compensation in DNA tracer concentration measurements, AIChE J. 65 (1) (2019) 40–48.
[53] C.A. Mora, D. Paunescu, R.N. Grass, W.J. Stark, Silica particles with encapsulated DNA as trophic tracers, Mol. Ecol. Resour. 15 (2) (2015) 231–241.
[54] L. Pang, B. Robson, E. McGill, A. Varsani, L. Gillot, J. Li, P. Abraham, Tracking effluent discharges in undisturbed stony soil and alluvial gravel aquifer using synthetic DNA tracers, Sci. Total Environ. 592 (2017) 144–152.
[55] V.R. Patel, Y. Agrawal, Nanosuspension: an approach to enhance solubility of drugs, J. Adv. Pharm. Technol. Res. 2 (2) (2011) 81.
[56] D. Paunescu, R. Fuhrer, R.N. Grass, Protection and deprotection of DNA—high-temperature stability of nucleic acid barcodes for polymer labeling, Angew. Chem. Int. Ed. 52 (15) (2013) 4269–4272.
[57] A.J. Pelley, N. Tufenkji, Effect of particle size and natural organic matter on the migration of nano-and microscale latex particles in saturated porous media, J. Colloid Interface Sci. 321 (1) (2008) 74–83.
[58] T. Phenrat, H.J. Kim, F. Fagerlund, T. Illangasekare, G.V. Lowry, Empirical correlations to estimate agglomerate size and deposition during injection of a polyelectrolyte-modified Fe0 nanoparticle at high particle concentration in saturated sand, J. Contam. Hydrol. 118 (3–4) (2010) 152–164.
[59] A.A. Porubcan, S. Xu, Colloid straining within saturated heterogeneous porous media, Water Res. 45 (4) (2011) 1796–1806.
[60] M. Puddu, D. Paunescu, W.J. Stark, R.N. Grass, Magnetically recoverable, thermostable, hydrophobic DNA/silica encapsulates and their application as invisible oil tags, ACS nano 8 (3) (2014) 2677–2685.

[61] Y. Qin, Z. Wen, W. Zhang, J. Chai, D. Liu, S. Wu, Different roles of silica nanoparticles played in virus transport in saturated and unsaturated porous media, Environ. Pollut. 259 (2020), 113861.
[62] T. Rahman, J. George, H.J. Shipley, Transport of aluminum oxide nanoparticles in saturated sand: effects of ionic strength, flow rate, and nanoparticle concentration, Sci. Total Environ. 463 (2013) 565–571.
[64] T. Raychowdhury, N. Tufenkji, S. Ghoshal, Aggregation and deposition kinetics of carboxymethyl cellulose-modified zero-valent iron nanoparticles in porous media, Water Res. 46 (6) (2012) 1735–1744.
[65] J.N. Ryan, M. Elimelech, Colloid mobilization and transport in groundwater, Colloids Surf. A Physicochem. Eng. Asp. 107 (1996) 1–56.
[66] I.H. Sabir, J. Torgersen, S. Haldorsen, P. Aleström, DNA tracers with information capacity and high detection sensitivity tested in groundwater studies, Hydrogeol. J. 7 (3) (1999) 264–272.
[67] M.B. Salerno, M. Flamm, B.E. Logan, D. Velegol, Transport of rodlike colloids through packed beds, Environ. Sci. Technol. 40 (20) (2006) 6336–6340.
[68] S. Sasidharan, S. Torkzaban, S.A. Bradford, P.G. Cook, V.V. Gupta, Temperature dependency of virus and nanoparticle transport and retention in saturated porous media, J. Contam. Hydrol. 196 (2017) 10–20.
[69] S. Sasidharan, S. Torkzaban, S.A. Bradford, P.J. Dillon, P.G. Cook, Coupled effects of hydrodynamic and solution chemistry on long-term nanoparticle transport and deposition in saturated porous media, Colloids Surf. A: Physicochem. Eng. Asp. 457 (2014) 169–179.
[70] J.F. Schijven, J. Šimůnek, Kinetic modeling of virus transport at the field scale, J. Contam. Hydrol. 55 (1–2) (2002) 113–135.
[71] J.F. Schijven, S.M. Hassanizadeh, R.H. de Bruin, Two-site kinetic modeling of bacteriophages transport through columns of saturated dune sand, J. Contam. Hydrol. 57 (3–4) (2002) 259–279.
[72] J.F. Schijven, S.M. Hassanizadeh, S.E. Dowd, S.D. Pillai, Modeling virus adsorption in batch and column experiments, Quant. Microbiol. 2 (1) (2000) 5–20.
[73] J. Shang, C. Liu, Z. Wang, Transport and retention of engineered nanoporous particles in porous media: effects of concentration and flow dynamics, Colloids Surf. A: Physicochem. Eng. Asp. 417 (2013) 89–98.
[74] X. Sheng-Hua, L. Yin-Mei, L. Li-Ren, S. Zhi-Wei, Computer simulation of the collision frequency of two particles in optical tweezers, Chin. Phys. 14 (2) (2005) 382.
[75] J. Šimůnek, M.T. Van Genuchten, M. Šejna, The HYDRUS software package for simulating two-and three-dimensional movement of water, heat, and multiple solutes in variably-saturated media, Tech. Man., Version 1 (2006) 241.
[76] T. Sugimoto, S. Hamamoto, T. Nishimura, Inhibited nanobubble transport in a saturated porous medium: effects of deposited colloidal particles, J. Contam. Hydrol. 242 (2021), 103854.
[77] H. Sun, R. Jiao, H. Xu, G. An, D. Wang, The influence of particle size and concentration combined with pH on coagulation mechanisms, J. Environ. Sci. 82 (2019) 39–46.
[78] P. Sun, A. Shijirbaatar, J. Fang, G. Owens, D. Lin, K. Zhang, Distinguishable transport behavior of zinc oxide nanoparticles in silica sand and soil columns, Sci. Total Environ. 505 (2015) 189–198.
[79] Y. Sun, B. Gao, S.A. Bradford, L. Wu, H. Chen, X. Shi, J. Wu, Transport, retention, and size perturbation of graphene oxide in saturated porous media: effects of input concentration and grain size, Water Res. 68 (2015) 24–33.
[80] Y. Tang, J.W. Foppen, T.A. Bogaard, Transport of silica encapsulated DNA microparticles in controlled instantaneous injection open channel experiments, J. Contam. Hydrol. 242 (2021), 103880.
[81] S. Torkzaban, S.M. Hassanizadeh, J.F. Schijven, H.A.M. De Bruin, A.M. de Roda Husman, Virus transport in saturated and unsaturated sand columns, Vadose Zone J. 5 (3) (2006) 877–885.
[82] S. Torkzaban, H.N. Kim, J. Simunek, S.A. Bradford, Hysteresis of colloid retention and release in saturated porous media during transients in solution chemistry, Environ. Sci. Technol. 44 (5) (2010) 1662–1669.
[83] S. Torkzaban, S.S. Tazehkand, S.L. Walker, S.A. Bradford, Transport and fate of bacteria in porous media: coupled effects of chemical conditions and pore space geometry, Water Resour. Res. 44 (2008) 4.
[84] M. Tourbin, C. Frances, Monitoring of the aggregation process of dense colloidal silica suspensions in a stirred tank by acoustic spectroscopy, Powder Technol. 190 (1–2) (2009) 25–30.
[85] N. Tufenkji, M. Elimelech, Correlation equation for predicting single-collector efficiency in physicochemical filtration in saturated porous media, Environ. Sci. Technol. 38 (2) (2004) 529–536.
[86] E. Vitorge, S. Szenknect, J.M. Martins, J.-P. Gaudet, Size-and concentration-dependent deposition of fluorescent silica colloids in saturated sand columns: transport experiments and modeling, Environ. Sci.: Process. Impacts 15 (8) (2013) 1590–1600.
[87] C. Wang, A.D. Bobba, R. Attinti, C. Shen, V. Lazouskaya, L.-P. Wang, Y. Jin, Retention and transport of silica nanoparticles in saturated porous media: effect of concentration and particle size, Environ. Sci. Technol. 46 (13) (2012) 7151–7158.
[88] Q. Xu, B. Ye, X. Mou, J. Ye, W. Liu, Y. Luo, J. Shi, Lead was mobilized in acid silty clay loam paddy soil with potassium dihydrogen phosphate (KDP) amendment, Environ. Pollut. 255 (2019), 113179.
[89] S. Xu, B. Gao, J.E. Saiers, Straining of colloidal particles in saturated porous media, Water Resour. Res. 42 (2006) 12.
[90] S. Xu, Q. Liao, J.E. Saiers, Straining of nonspherical colloids in saturated porous media, Environ. Sci. Technol. 42 (3) (2008) 771–778.
[91] H. Yang, M. Tong, H. Kim, Effect of carbon nanotubes on the transport and retention of bacteria in saturated porous media, Environ. Sci. Technol. 47 (20) (2013) 11537–11544.
[92] R. Yuan, W. Zhang, X. Tao, S. Wang, L. Zhang, Coupled effects of high pH and chemical heterogeneity on colloid retention and release in saturated porous media, Colloids Surf. A: Physicochem. Eng. Asp. 586 (2020), 124285.
[93] Y. Zhang, M.B. Hartung, A.J. Hawkins, A.E. Dekas, K. Li, R.N. Horne, DNA tracer transport through porous media—the effect of DNA length and adsorption, Water Resour. Res. 57 (2) (2021), 2020WR028382.